IAA-AAS-DyCoSS2-14-05-07

PERFORMANCE CHARACTERISTICS OF THE UWE-3 MINIATURE ATTITUDE DETERMINATION AND CONTROL SYSTEM

Philip Bangert,[*] Stephan Busch,[†] and Klaus Schilling[‡]

Modern miniaturization techniques enable the realization of 3-axis attitude determination and control systems (ADCS), appropriate for the 1 kg pico-satellite class. One of the most challenging aspects concerns the support for continuous ADCS operations at reasonable accuracies despite extremely limited resources available on small satellite platforms. The very low power ADCS of the pico-satellite UWE-3 is based on miniature Sun sensors, magnetometers and MEMS sensors for attitude determination to control the satellite using six magnetic torquers and a single reaction wheel. After successful launch in November 2013, the main technical objective of the third UWE satellite is currently the in-orbit demonstration and characterization of its attitude determination and control capabilities. This contribution addresses the system design aspects and provides results obtained during its first months of operation.

INTRODUCTION

One of the most promising applications of pico-satellites has as objective joint observations by coordinated multi-satellite missions. For this task, adequate attitude determination and control is a crucial requirement. One of the challenges for pico-satellites (at a total mass of about 1 kg) is the realization of a suitable 3-axis attitude control system. Pico-satellites typically have very limited resources in energy, mass and size. Thus, the ADCS on most of the early pico-satellites used passive control and offline analysis of attitude determination sensor data.

Only few pico-satellite projects achieved to demonstrate on-board attitude determination and active attitude control while various missions could not validate the performance of the ADCS for various reasons.[4, 11] Most of the available systems rely on magnetic actuators for attitude control. Demonstrated control capabilities of miniature satellites still provide only rough accuracies compared to larger spacecraft.[2] The utilization of miniature reaction wheels on pico-satellites such as demonstrated on the BEESAT[5] mission is still limited to short-duration operations of a single wheel due to excessive power consumption.

The state of the art is documented for example in a NASA survey[7] or in [12], stating that accuracies in attitude determination of a few degrees could be achieved by nano-satellites such as CanX-2, which has been equipped with fine sun-sensors.[9] However, challenges in the pico-

[*] MSc, Informatics VII: Robotics & Telematics, University Würzburg, 97074 Würzburg, Germany
[†] Dipl.-Inf. MSc, Informatics VII: Robotics & Telematics, University Würzburg, 97074 Würzburg, Germany
[‡] Prof. Dr., Zentrum für Telematik, 97218 Gerbrunn, Germany.

satellite class are even more demanding as sensors involved have to be extremely small, light-weight, and efficient to allow continuous operation of the system. The utilization of high precision sensors such as star trackers is still so far not feasible.

Following the vision to realize a cooperating formation of pico-satellites within this decade the University of Wuerzburg established a roadmap targeting the development and demonstration of corresponding enabling technologies.[8] Since 2005, three pico-satellites have already been launched in the context of the University of Wuerzburg Experimental satellite (UWE) program. UWE-1, the first German pico-satellite had the main objective to establish a robust communication link based on Internet Protocols to the ground segment.[1] Launched in 2009, UWE-2 was carrying a preliminary attitude determination sensor suite as an extension of the UWE-1 platform. Recently, in late 2013 the a new generation of UWE satellites has been launched to demonstrate real-time attitude determination and first attitude control capabilities in-orbit. As an extension of the UWE-3 platform, UWE-4 will demonstrate a miniature electrical propulsion system[6] for future formation control, which is planned to be realized in a 4 vehicle formation with UWE-5 to UWE-8.

Besides the development of a low power ADCS with UWE-3 (see Figure 1) an innovative generic pico-satellite architecture has been introduced in order to constitute a robust and flexible base for the upcoming UWE missions.[3] The key design driver was to achieve a very low power consumption of the COTS-based system, while maintaining a robust and fully functional miniature satellite. Further, the generic design is optimized to support robust and rapid development, integration and testing of the satellite as well as easy maintenance, extension and replacement of subsystems in any configuration during development or integration.

In order to achieve a consistent realization of the mentioned aspects all subsystems of the satellite have been designed by the team in Wuerzburg. UWE-3 features

- a dual-redundant low power on-board computer,
- a redundant and scalable distributed electrical power system,
- a fully redundant UHF communication system and
- an attitude determination and control system being capable of operating continuously the ico-satellite.

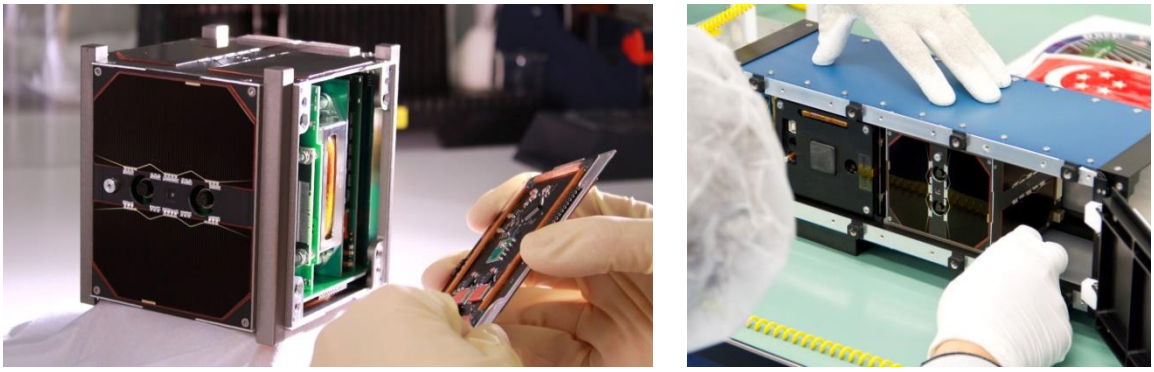

Figure 1: UWE-3 Flight Model during integration campaign (left). Integration of UWE-3 into the satellite deploymen system (right) later mounted on the Dnepr Space Head Module.

THE ATTITUDE DETERMINATION AND CONTROL SYSTEM DESIGN

The UWE-3 Attitude Determination and Control System is built on a standard UWE-3 subsystem board and uses a MSP430.[10] The sensor suite consists of three types of sensors: magnetometers, sun-sensors, and gyroscopes. Attitude Control is mainly achieved with magnetic torquers realized as air-coils mounted on the inside of each panel (see Figure 2, right). Additionally, the satellite carries a miniaturized reaction wheel, intended for fast slew maneuvers.

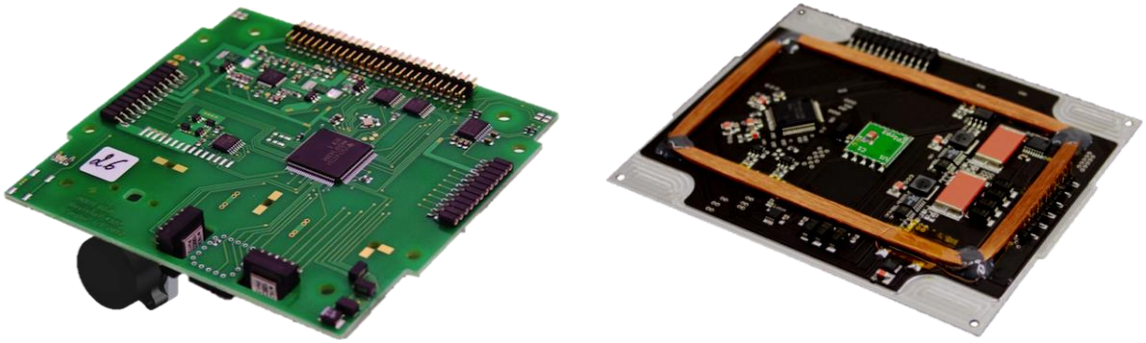

Figure 2: UWE-3 low power ADCS (left). UWE-3 multifunctional side panel with sun sensor, magnetometer and magnetic troquer (right)

The magnetometers are surface mounted single-axis hall sensor devices of which in total nine sensors are distributed within the satellite resembling three complete 3-D compasses. The primary set of sensors is located on the ADCS board (see Figure 2, left) itself while the secondary sets are mounted with one sensor on each panel of the satellite (see Figure 2, right). Although located inside the CubeSat, the achievable precision for 3D magnetometer measurements has been proven to be better than 3 deg.

The sun-sensors are located in the center of each panel and measure two angles towards the brightest object within a large FOV of 150°. The optoelectronic low power ASIC devices are capable of determining the direction of incident light with an angular resolution of 2.7 deg and an accuracy of about 5 deg. Furthermore, they provide a measurement of the incident light intensity which is used to discriminate between the sun and other objects within their FOV such as the Earth's albedo.

The gyroscopes are single-axis MEMS devices mounted on the ADCS PCB orthogonally to each other. They can measure the satellite's angular rate up to 320 deg/sec with a resolution of 0.073 deg/sec and a typical noise of 0.15 deg/sec. Even though the sensors provide internal temperature compensation they can experience temperature related drifts which have to be estimated by the Kalman filter.

The attitude sensor information is fused using an Isotropic Kalman filter. Different modes are available for optimizing the ADCS power consumption, mainly characterized by the duty cycle of the gyroscopes. In low power mode the gyroscopes are only activated for a very short period, reducing the overall power consumption to a third. However, in this mode the sensor noise level is highly increased, rendering additional digital filtering necessary.

The magnetic air coils are of the dimensions 52 x 85 mm², have 300 windings and a maximal voltage of +/- 3.8 V can be applied. Each coil can produce a magnetic moment of 0.028 Am² and all six of them are operated in parallel giving a total maximum magnetic moment $\mu_{max} = 0.1\ \mathrm{Am}^2$. With a maximal Earth magnetic field of $B_{max,\ Earth} = 46\ \mu T$ the ADCS can produce

magnetic torques up to $T_{\max} = \mu_{max} \times B_{max,Earth} = 4.6 \cdot 10^{-6}\, Nm$ and using the reaction wheel a maximum torque of $2.3 \cdot 10^{-5}\, Nm$.

Besides a single axis wheel controller for fast slew maneuvers, different magnetic attitude control laws have been implemented. The B-Dot Controller is used for actively damping the satellite's rotation by applying a torque opposite to the direction of the current change of the measured magnetic field. A Follow B-Field Controller applies a constant magnetic moment on one axis and operates as damping controller on the other two axes. This results in an alignment of one satellite body axis with the external magnetic field. Last, an experimental COMPASS Controller aims to align the satellite's body reference frame with the orbital reference frame, resulting in a nadir pointing of the satellite.

The attitude control is activated only during a fraction of the time according to an adjustable duty cycle. This has been implemented in order to save power as well as to avoid the loss of the satellite in case of a malfunction of one of the torquers. Especially during first operations it was used as a safety precaution in case the activation of a torquer would disturb the communication link.

During ground testing attitude determination accuracies on the order of 5 deg could be demonstrated, mainly limited by the inaccuracies in the test facility (magnetic field irregularities) and the sun-sensor's resolution. Attitude control using the magnetic torquers was demonstrated on ground during detumbling experiments.[10]

During nominal operations the ADCS consumes about 60 mW (including external sensors) which adds up to a total power consumption of the satellite of about 350 mW. In this mode the sampling rate of the MEMS gyros is reduced to 0.1 Hz which is sufficient for slow dynamics. In high precision determination mode with fast gyro sampling the power consumption is about 400 mW. The additional power consumption of the magnetic torquers is max. 540mW depending on the duty cycle. When reaction wheel control is used with high precision determination mode the total power consumption of the satellite is about 1200 mW.

IN-ORBIT PERFORMANCE ANALYSIS

The UWE-3 satellite has been launched from Yasny, Russia, on November 21, 07:10 UTC on board a Russian DNEPR rocket. After first contact with the ground station in Würzburg at 08:51 UTC the commissioning phase started focusing mainly on monitoring the satellite's health status. On December 3rd the ADCS was turned on for the first time. Although the satellite has continuously been in a very good health state with batteries charged above 80% in general, the ADCS was set into power saving mode in order to monitor the satellite's initial motion before applying any control mode.

The satellite initially was spinning at a rate of approximately 23deg/s about an arbitrary axis. Different features were visible in the motion, such as external torques (presumably due to a residual magnetic moment within the satellite) and a natural damping. In order to characterize and evaluate the active damping with the magnetotorquers, an analysis of the natural spin decay was carried out over several days. The results are shown in Figure 3 where the spin rate measured with the gyroscopes is shown from the time the ADCS was switched on for the first time until shortly after having applied the B-Dot controller. The natural damping rate was found to be about 0.5deg/s per day.

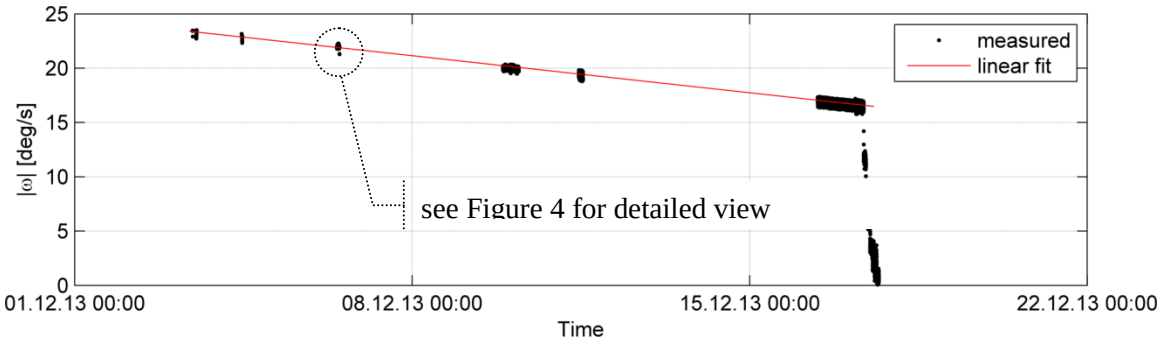

Figure 3: Spin rate decay due to natural damping and subsequent active detumbling.

Furthermore, an analysis of the satellite's rotation axis reveals that there are external torques present that periodically change the rotation axis as shown in Figure 4. Efforts to characterize these torques are ongoing in order to estimate their magnitude and origin.

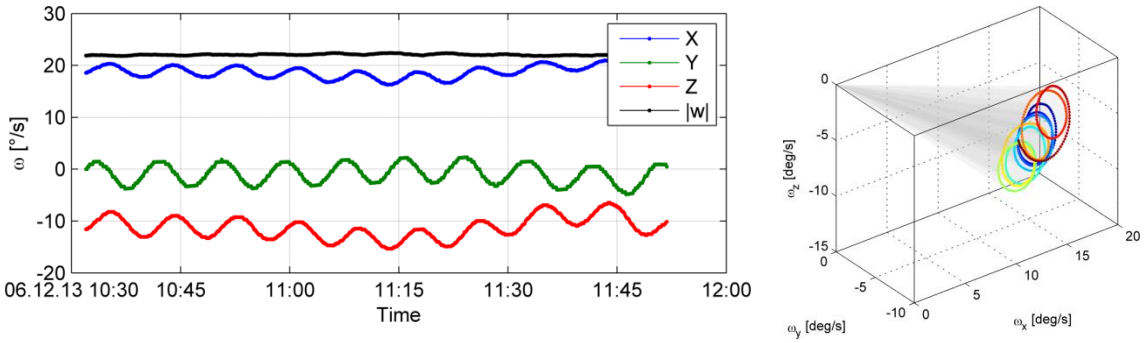

Figure 4: Varying rotation axis of tumbling satellite due to external torques shown as rate vector components (left) and corresponding 3D trace (right).

After having gathered more than 300 kBytes of data for the natural damping analysis the ADCS was switched into B-Dot control mode in order to actively detumble the satellite. As mentioned above, the control moments are activated according to a duty cycle which has been set to 1 minute within 10 minutes. The actual spin rate was measured throughout the operation and the control mode was kept active for one orbit (97 minutes). Shown in Figure 5 is the rotational speed of the satellite during this orbit where also the torque activation periods are clearly visible. The satellite was slowed down from its initial rate of 16.5deg/s to about 1deg/s within 7 minutes of activated control torque. It can be seen that the rotation rate about all axes decreases evenly which indicates that the satellite was able to produce control torques in all three axes over the course of one orbit.

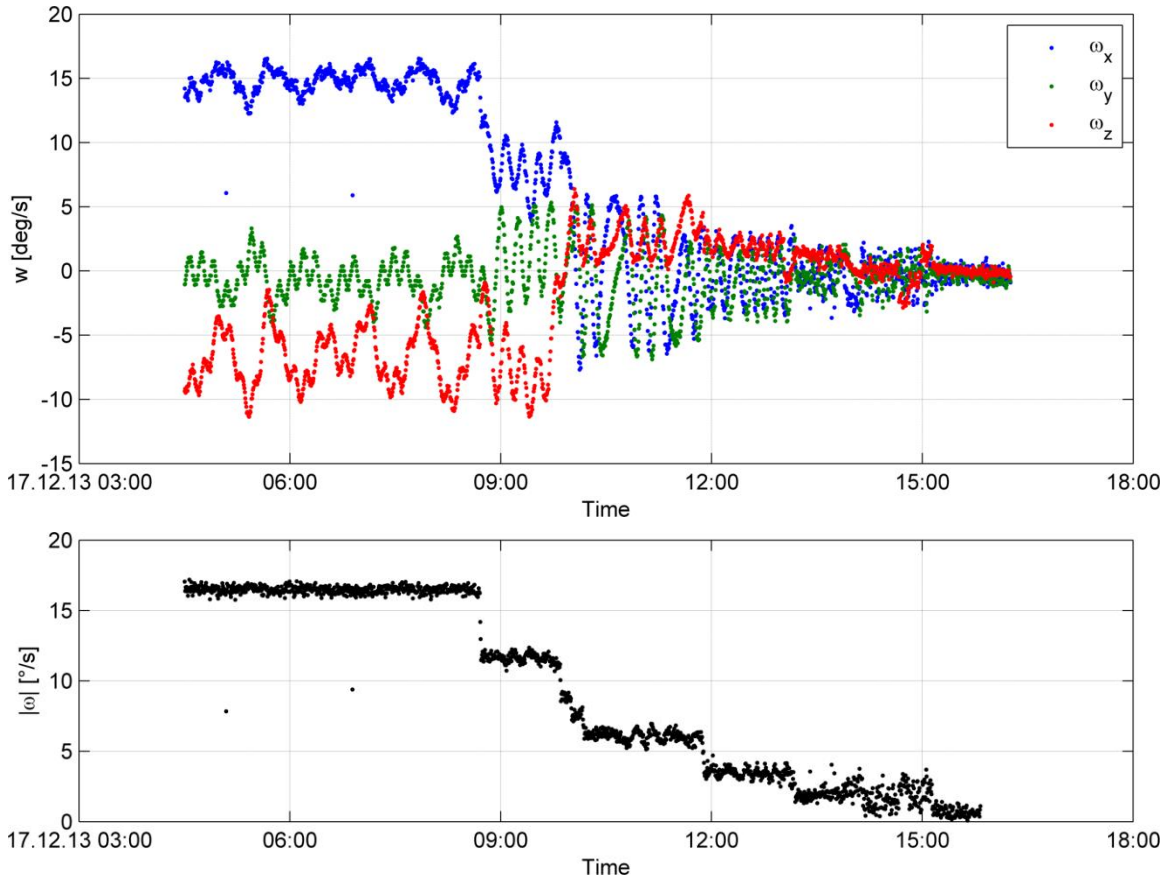

Figure 5: Satellite motion during active detumbling.

The detumbling process has been visualized in Figure 6 where the rate vector is shown as 3D trace in different perspectives. The color indicates the progressed time, starting from dark blue on Dec. 17th 4:30h and ending with dark red on Dec. 17th 15:45h. Clearly visible are the oscillation due to precession and the different stages of detumbling during the process. Also a change in the precession axis can be identified.

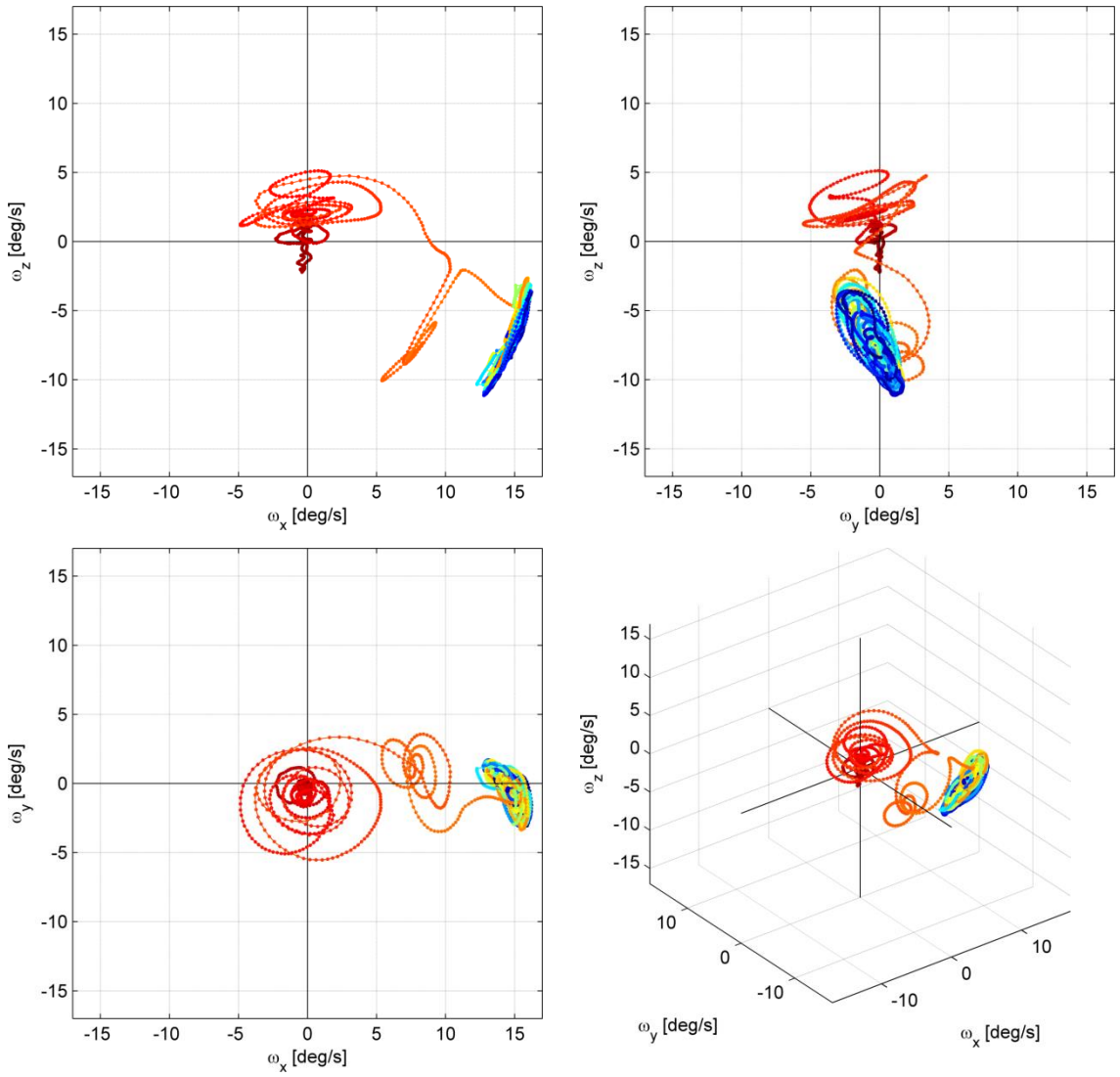

Figure 6: 3D trace of rotation axis during active detumbling based on the same data set as shown in Figure 4. The color indicates the progressed time, starting with dark blue on Dec 17th 4:30h.

Attitude Determination Performance

A performance analysis of the attitude determination is possible by comparing the satellite's different absolute sensor measurements (magnetometer and sun-sensors) with their corresponding reference models in ECI coordinates. The satellite records the sensor measurements in its own body coordinate frame and estimates its attitude providing a quaternion describing the coordinate transformation between ECI coordinates and the body coordinate frame. Using these recordings from the satellite, one can transform the measurements into ECI frame to compare them to the official reference models such as the IGRF-11 for the magnetic field.

The comparison then includes different sources of inconsistencies, such as the sensors' noise, minor inaccuracies of the models and calibration inaccuracies. However, the overall match of the

transformed measurements and their corresponding reference models gives a worst case estimation of the satellite's absolute attitude determination accuracy.

Such an analysis was carried out on Dec. 19th, where within 121 minutes 1354 sets of quaternions, 1354 magnetic field measurements, 425 sun measurements and 207 gyroscope measurements have been recorded. The magnetic field measurements and sun-vectors were transformed into ECI coordinates and compared to the models, as shown in Figure 7. Obviously, the matching is not accurate and a mean deviation from the measurements and the model can be found in Table 1.

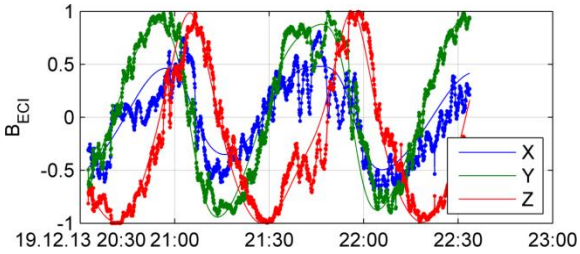

Figure 7: Magnetic field measurement before calibration transformed to ECI

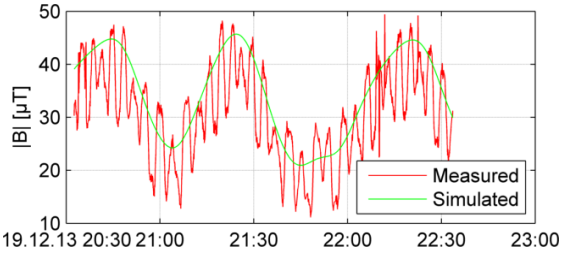

Figure 8: Measured magnetic field strength before calibration

From these findings it became obvious that the attitude determination was not correctly adjusted and that accuracy as shown during tests had not been achieved yet. The reason for this was shortly after found while studying the magnetic field measurements and in particular the magnetic field strength. It is shown in Figure 8 that the measured field strength oscillated according to the satellite's rotational motion rather than only due to its orbital motion. This effect indicated that the magnetometers were not calibrated correctly.

Table 1: Angular deviations of sensor measurements from predicted reference models before calibration.

	Deviation with 99% confidence interval
Magnetic Field measurements	[1.59 < 15.01 < 35.57] deg
Sun vector	[0.83 < 9.22 < 35.09] deg

In-Orbit Calibration

The in-orbit calibration of the magnetometers was achieved by analyzing the measured magnetic field strength. This quantity is invariant to rotations of the satellite and thus only changes over the course of one orbit. The task is now to find a calibrated magnetic field measurement $\widetilde{\boldsymbol{b}}$ that matches the reference magnetic field strength $|\boldsymbol{b}_{\boldsymbol{model}}|$ at all times and thus under all rotations of the satellite. The only requirement to apply this procedure is that the satellite is not entirely stabilized about an axis but rotates about all three axes with respect to the Earth magnetic field such that the magnetic field strength measured along one axis changes over time.

Using standard minimization algorithms a calibration matrix $\boldsymbol{C}$ (taking into account gain and cross-axis effects) and offset $\boldsymbol{\mu}$ can be found such that the measured magnetic field $\boldsymbol{b}$ can be corrected to produce the calibrated magnetic field $\widetilde{\boldsymbol{b}} = \boldsymbol{C} * (\boldsymbol{b} - \boldsymbol{\mu})$ while minimizing the error func-

tion $E = abs(|\tilde{\boldsymbol{b}}| - |\boldsymbol{b_{model}}|)$. Currently, an analysis is being carried out to find a stable error function based in the frequency domain, which would render the use of external information such as the satellite's position and the reference magnetic field dispensable. The calibration found was

$$\boldsymbol{\mu} = \begin{bmatrix} -6.161 \\ 4.885 \\ 4.045 \end{bmatrix}$$

$$\boldsymbol{C} = \begin{bmatrix} 1.140 & -0.066 & -0.041 \\ 0.063 & 1.141 & 0.013 \\ 0.037 & -0.079 & 1.081 \end{bmatrix}$$

and was uplinked on Jan. 23rd.

Figure 9 (a) shows the result of this calibration for the mentioned data recording. In the figure on the left the magnetic field strength is shown over time. Shown in red is the field strength as measured by the uncalibrated magnetometers, in blue the measurements after the correct calibration is applied and in green the magnetic field strength of the IGRF-11 model. We can see, that the uncalibrated field strength not only varies due to the orbital movement (slow variation) but oscillates according to the rotational movement of the satellite. This component vanishes when the calibration is applied to the raw data, as can be seen in the blue graph.

Shown in Figure 9 (b) is the distribution of the deviation of the magnetic field strength from the IGRF-11 reference field for all data recordings until March 4th (more than 52.000 data points). Again, shown in red is the uncalibrated raw data and in blue the data after applying the found calibration based on the data from Dec. 19th. It is visible that the calibrated measurements form a narrow distribution with the center almost at zero µT deviation while the raw data shows a wide distribution with an offset of 4.5 µT. The distribution characteristics are shown in Table 2.

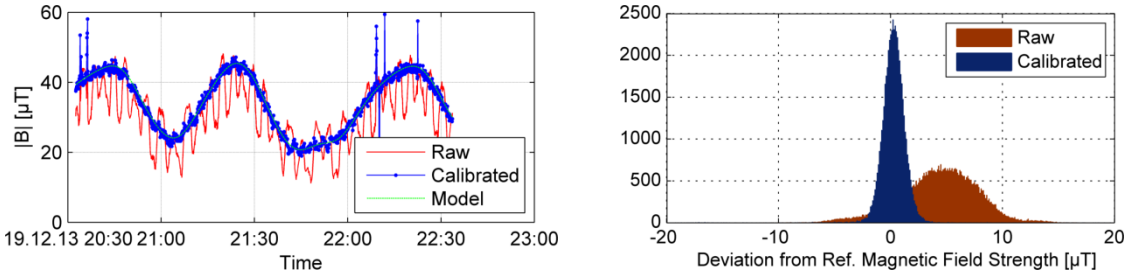

(a) (b)

Figure 9: Magnetig field strength before and after sensor calibration compared to the IGRF-11 reference model data.

Table 2: Magnetic field strength deviation of magnetometer measurements from predicted reference models before and after calibration

	Magnetic field strength deviation with 95% confidence interval
Raw	[-1.80 < 4.56 < 9.46] µT
Calibrated	[-1.30 < 0.25 < 1.80] µT

Until today, more than 52.000 magnetic field measurements have been recorded giving the opportunity to create magnetic field maps as shown in Figure 10 where also the IGRF-11 refer-

ence magnetic field model is shown. Despite the use of the magnetic torquers and the reaction wheel, this calibration has been found to be valid and only minor deviations of less than 3% of the magnetic field strength are measured. However, an increase in accuracy can be expected when the calibration procedure is applied to the complete magnetic field measurements gathered so far, which is currently being prepared.

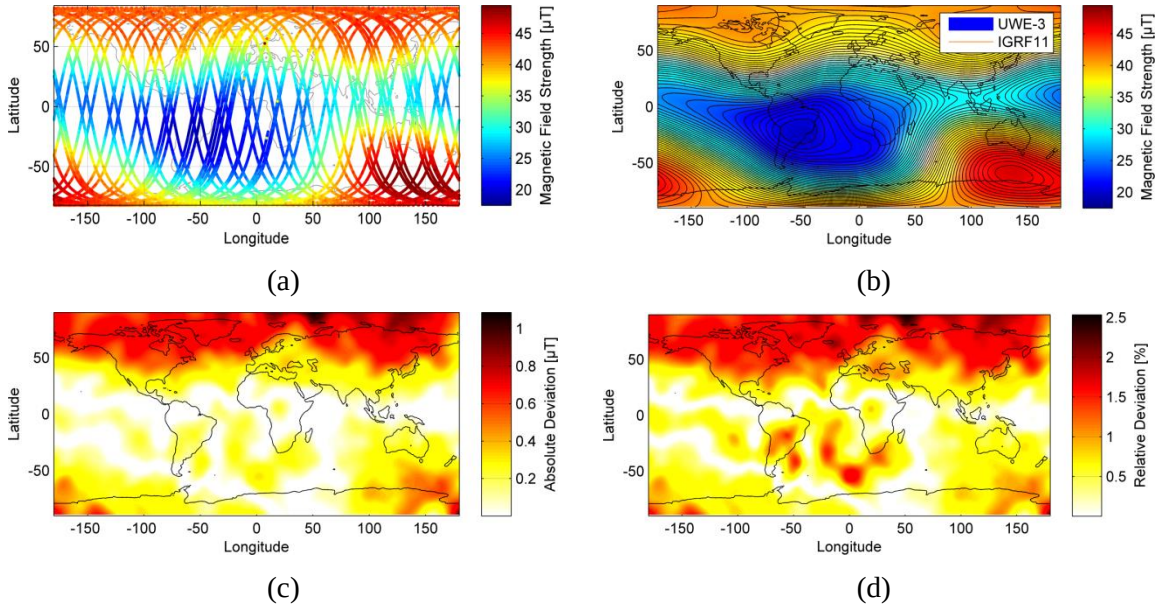

Figure 10: Calibrated magnetic field strength as measured during several orbits (a) compared to the reference model IGRF-11 as overlay (b), absolute deviation (c) and relative deviation (d).

Deviations can mainly be seen in regions such as the magnetic poles and the south-Atlantic anomaly where the Earth's magnetic field undergoes changes due to the solar wind and seasonal variations.

Attitude Determination After In-Orbit Calibration

Having calibrated the magnetometers, the attitude determination was characterized again using data recorded on Jan. 27th. The obtained magnetic field transformed into ECI coordinates using the quaternions and their corresponding reference vectors are shown in Figure 12. The accuracy of the measurements is shown in Table 3. It should be noted, that these accuracies give a worst case estimate of the attitude determination since they still include the sensor noise on top of the attitude estimation noise. It should be noted that for the sun-sensors there has not been performed a dedicated in-orbit calibration yet, causing a higher maximal deviation. However, the mean deviation between the measured sun-vector in ECI frame and the reference vector is only 0.2 deg.

Also visible in the data of the sun-sensors is the eclipse, where no sun-sensor measurements are shown. During this time the attitude determination is purely based on the magnetic field measurements and attitude predictions based on the gyroscopes and is therefore missing information about one rotational axis (about the magnetic field direction). However, after exiting the eclipse the satellite acquires valid sun-sensor data again. The first few measurements show a

slightly higher mismatch until the necessary adjustments to the estimated attitude are made by the Kalman filter.

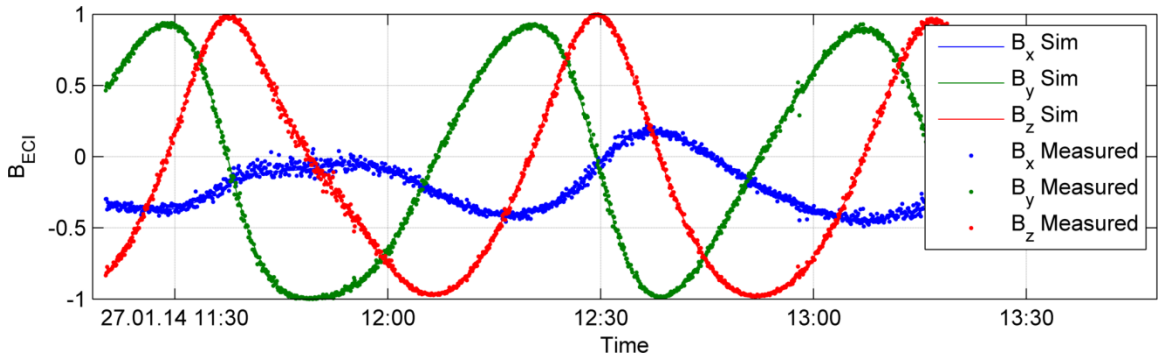

Figure 11: Magnetic field measurement after calibration transformed to ECI, compared with simulated reference model (compare Figure 7 without calibration).

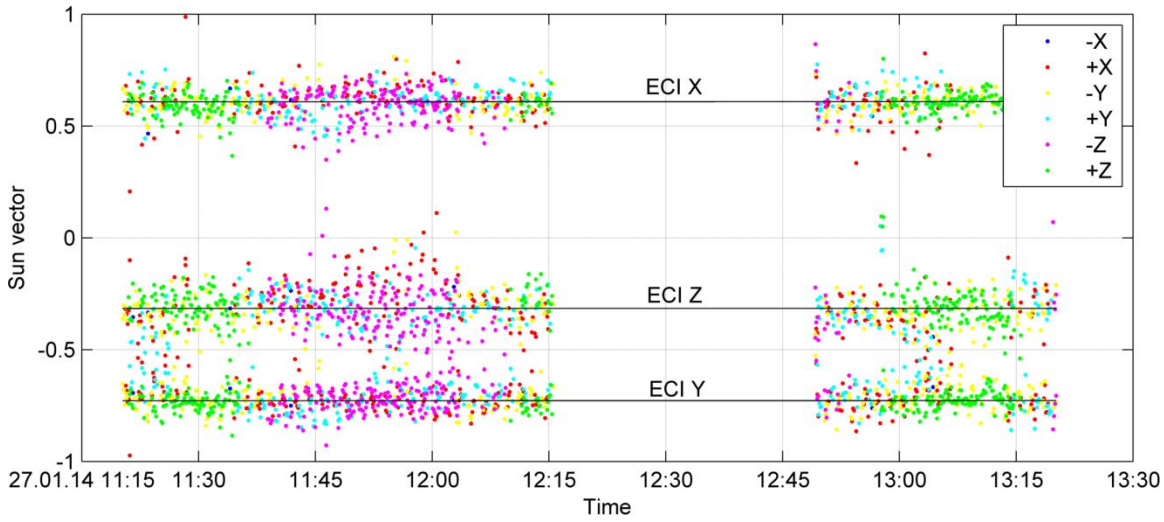

Figure 12: Sun vector measurements of all 6 Sun sensors (uncalibrated) transformed to ECI coordinates and compared with expected Sun vector.

Table 3: Angular deviations of sensor measurements from predicted reference models after magnetometer calibration.

	Deviation with 99% confidence interval
Magnetic Field measurements	[0.17 < 1.83 < 6.03] deg
Sun vector	[0.51 < 3.79 < 11.93] deg

Natural Motion after Detumbling

The satellite's motion without active control has been analyzed after in-orbit calibration and it was found that the satellite is passively stable with respect to the Earth's magnetic field. This can

be seen in Figure 13 where the direction of the magnetic field in Body coordinates is shown for different recordings each covering at least one full orbit. The first row (Dec 09th) shows the state before active detumbling of the satellite whereas the following figures show the evolution of the state after detumbling. It is clearly visible that before the satellite's rotation was actively slowed down magnetic field directions could be measured in all axes whereas afterwards the magnetic field has been measured predominantly in the negative Z direction with this preference becoming more and more prevailing with time. This effect presumably is due to a residual magnetic dipole directed along the negative Z axis which tends to align the satellite with the Earth's magnetic field.

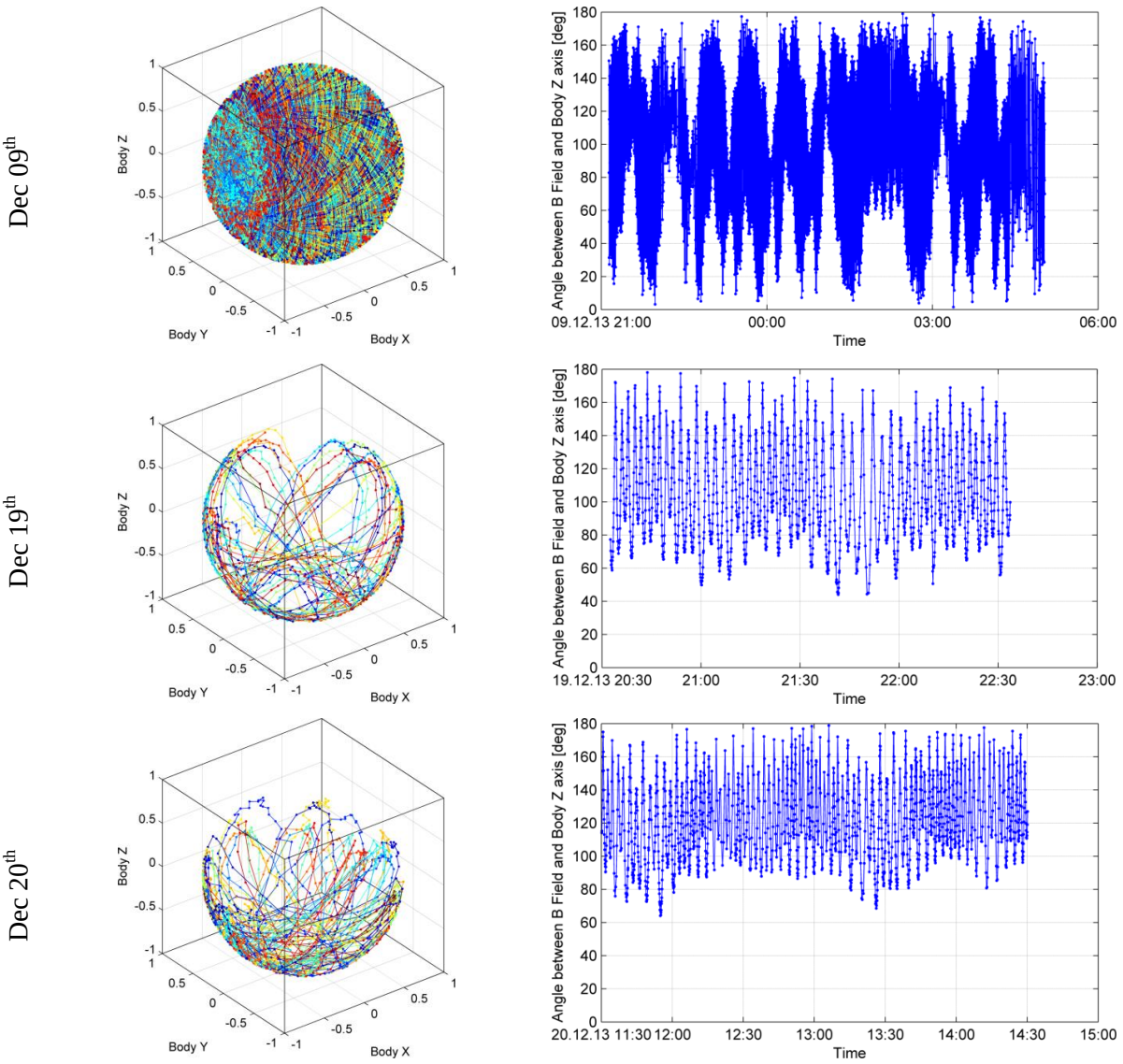

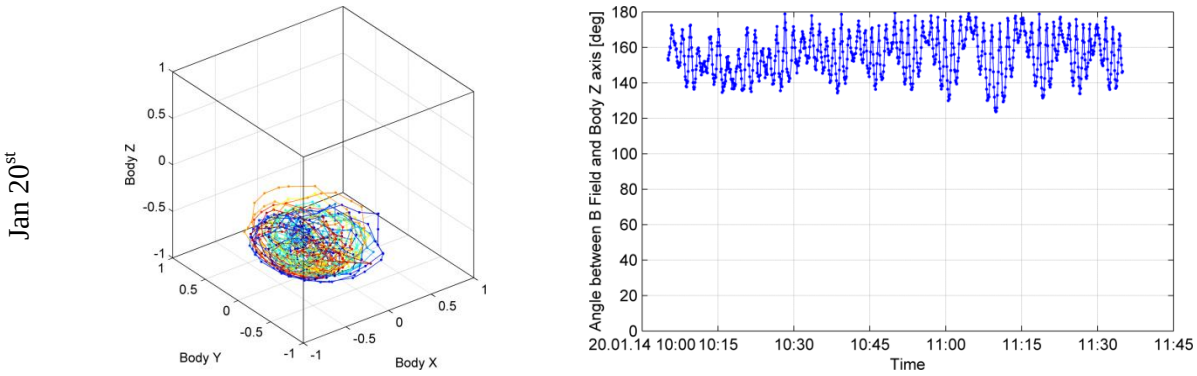

Figure 13: Magnetic field direction in body frame (left colum) and its alignment with the satellite's Z-axis (right colum) over time, before active detumbling (Dec 09th), and its passive progression after active detumbling (Dec 19th – Jan 20th)

CONCLUSIONS

The design approach to the attitude determination and control system of the pico-satellite UWE-3 was presented, as well as the results from preliminary in-orbit performance tests. The analysis of the low power attitude control system based on 6 magnetic torquers and one reaction wheel has been conducted in the first three month of operation after launch in November 2013.

After in-orbit calibration of the magnetic sensor suite, the magnetic field strength measurements showed only minor deviations in the order of 3% of the magnetic field strength compared to the corresponding IGRF-11 reference data. Using the attitude estimation by the on-board Kalman-filter the measurements of sun sensors and magnetometers were compared to the corresponding reference model. The results demonstrate an excellent performance of the miniature devices mounted inside the pico-satellite. An attitude estimation accuracy on the order of a few degrees could be achieved after calibration of the magnetometers. Higher accuracies are expected after calibration of the complete sensor suite.

The initial tumbling rate after separation of about 16 deg/s could be decelerated to less than 1 deg/s by active damping within a few minutes using the magnetic torquers. Continuous operation of the ADCS appears feasable with the satellite's power budget.

The UWE-3 system exhibits very good health after 3 months in orbit, such that future operations will target the optimization of the attitude determination and control system by improving the sensor calibrations as well as adjusting the noise factors for the Kalman filter. The presented analysis will be carried on in order to further characterize the performance. Moreover, different attitude control modes are to be tested including attitude control using the reaction wheel and combined magnetic and wheel controllers.

ACKNOWLEDGMENTS

The authors acknowledge the funding for UWE-3 by the Federal Ministry of Economics and Technology, following a decision of the German Bundestag, via the German Aerospace Center (DLR) with funding grant number 50 RU 0901.

REFERENCES

[1]R. Barza, Y. Aoki, K. Schilling. *CubeSat UWE-1 Technology Tests and In Orbit Results*. In 57th International Astronautical Congress Valencia, IAC-06-B5.3.07, 2006.

[2]J. Bouwmeester, J. Guo, *Survey of worldwide pico- and nanosatellite missions, distributions and subsystem technology*, ActaAstronautica, Vol. 67, pp. 854–862, 2010991

[3]S. Busch, P. Bangert, F. Reichel, K. Schilling; *The UWE Satellite Bus, a Modular and Flexible Architecture for Future Picosatellite Formations*, 64. IAC Congress, Beijing, China. 2013

[4]K. Fujiwara, K. Omagari, T. Iljic, S. Masumoto, Y. Konda, T. Yamanaka, Y. Tanaka, M. Maeno, T. Ueno, H.i Ashida, J. Nishida, T. Ikeda, S. Matunaga, *Tokyo Tech Nano-Satellite Cute-1.7+APD Flight Operation Results and the Succeeding Satellite*, 17th IFAC Symposium on Automatic Control in Aerospace, Toulouse, France, June 25-29, 2007

[5]M. Herfort, M. Berlin, H.-P. Geile, Z. Yoon, "BeeSat Attitude Determination and Control System," Proceedings of the 6th IAA Symposium on Small Satellites for Earth Observation, Berlin, Germany, April 23 - 26, 2007

[6]I. Kronhaus, M. Pietzka, K. Schilling, J. Schein. *Picosatellite Orbit Control by Vacuum Arc Thrusters as Enabling Technology for Formation of Small Satellites*. In 5th International Conference on Spacecraft Formation Flying Missions and Technologies, 2013.

[7]Mission Design Division Staff, Ames Research Center, *Small Spacecraft Technology State of the Art*, NASA/TP–2014–216648, February 2014

[8]M. Schmidt, K. Schilling. *Formation Flying Techniques for Pico-Satellites.* In 6th International Workshop on Satellite Constellation and Formation Flying, IWSCFF-Paper-2010-3-5 2010.

[9]D. Rankin, D. Kekez, R. Zee, F. Pranajaya, D. Foisy, a Beattie. *The CanX-2 nanosatellite: expanding the science abilities of nanosatellites.* Acta Astronautica, 57 (2–8) (2005), pp. 167–174

[10]F. Reichel, P. Bangert, S. Busch, K. Ravandoor, K. Schilling: *The Attitude Determination and Control System of the Picosatellite UWE-3*, 19th IFAC Symposium on Automatic Control in Aerospace, Würzburg, Germany, September 2013.

[11]A. Scholz, W. Ley, B. Dachwald, J.J. Miau, J.C. Juang, *Flight results of the COMPASS-1 picosatellite mission,* Acta Astronautica 67 (2010) 1289–1298.

[12]D. Selva, D. Krejci, *A survey and assessment of the capabilities of Cubesats for Earth observation*, Acta Astronautica, 74 (2012) 50–68.